Functional MRI Study of Alzheimer's and Cognitive Normal Elderly Subjects

By

Yuchen Wu

Thesis

Submitted to the Faculty of the

Graduate School of Vanderbilt University

in partial fulfillment of the requirements

for the degree of

MASTER OF SCIENCE

in

Electrical Engineering

August 31, 2020

Nashville, Tennessee

Approved:
D. Mitchell Wilkes, Ph.D.
Richard A. Peters, Ph.D.

Table of Contents

Page

List of Figures 1

Chapter

I. Introduction 1

1. Related Works on fMRI Analysis 1
2. Introduction to Alzheimer's Disease 2
3. Introduction to Cognitive Normal Elderly 3
4. K-means Algorithm 4
5. Markov Chains 5
6. Sliding Window PCA 5

II. Methods 9

1. Data Collection 9
2. Preprocessing of Raw Data 10
3. Data Analysis 11

III. Results 14

1. Preprocessing 14
2. Clustering 15
3. Markov Chain Model 18
4. CAP Analysis 22
5. Sliding Window PCA 28

IV. Discussion 33

1. Clustering 33
2. Markov Chain Model 33
3. CAP Analysis 34
4. Sliding Window PCA 34

V. Conclusions 35

References 36

List of Figures

Figure **Page**

1. Original structural MRI image of AD subject 006_S_4153 14

2. Skull-removed structural MRI image of AD subject 006_S_4153 in MNI space 15

3. Clustering result of AD subject 002_S_5018, k=10 16

4. Clustering result of AD subject 002_S_5018, k=6 16

5. Clustering result of AD subject 003_S_6264, k=10 17

6. Clustering result of CN subject 002_S_0295, k=10 17

7. Clustering result of CN subject 002_S_0413, k=10 18

8. Markov chain result of AD subject 002_S_5018, k=10.....19

9. Markov chain result of AD subject 002_S_5018, k=6.....20

10. Markov chain result of CN subject 002_S_0295, k=10.....21

11. Markov chain result of CN subject 002_S_0413, k=10.....22

12. Spatial CAP result of AD subject 002_S_5018, k=10 23

13. Temporal CAP result of AD subject 002_S_5018, k=10 24

14. Spatial CAP result of AD subject 003_S_6264, k=10 25

15. Temporal CAP result of AD subject 003_S_6264, k=10 26

16. Spatial CAP result of CN subject 002_S_0295, k=10 27

17. Temporal CAP result of CN subject 002_S_0295, k=10 28

18. IWBC of AD subject 130_S_4982.....29

19. Sliding window result of AD subject 130_S_4982 for timepoint 21.....30

20. Sliding window result of AD subject 130_S_4982 for timepoint 50.....30

21. IWBC of CN subject 037_S_0303.....31

22. Sliding window result of CN subject 037_S_0303 for timepoint 115 31

23. Sliding window result of CN subject 037_S_0303 for timepoint 158 32

24. Sliding window result of CN subject 037_S_0303 for timepoint 174 32

Chapter I. Introduction

Functional magnetic resonance imaging (fMRI) is widely used to study the characteristics of the human brain activities. Most of the analysis methods are based on voxels. Some summary statistics characterizing the temporal response in each voxel are computed and represented in the spatial domain by a brain map for visual inspection or additional inference (see, e.g., Bandettini et al., 1993; Worsley and Friston, 1995; Xiong et al., 1996; and Lange and Zeger, 1997). This method usually relies on some model and assumption about the fMRI acquisition, e.g., concerning the stimulus, the haemodynamic response, among others. This work attempts to explore the avalanches of resting-state fMRI via K-means clustering, the co-activation pattern (CAP) analysis, Markov chains and sliding window principle components analysis (PCA) in Alzheimer's disease (AD) and cognitive normal (CN) subjects. The K-means clustering is used to establish states for the Markov chain. Different brain activation patterns among Alzheimer's disease (AD) and cognitive normal (CN) subjects can be found according to the analysis. These findings suggest that functional neuroimaging can be used as a method of identifying pre-clinical Alzheimer's disease.

1. Related Works on fMRI Analysis

A traditional fMRI analysis method focuses on describing the relationship between cognitive variables and individual brain voxels (volumetric pixels). This approach is proved to be tremendously productive. However, there are limits on what we can learn from cognitive states by examining voxels in isolation.

A recent approach on neuroimaging using fMRI relies on exploratory data analysis (EDA). Different from principal component analysis (PCA) (Sychra et al., 1994) and recent developments

in independent component analysis (ICA) (Mckeown et al., 1998), EDA in neuroimaging is applied using clustering methods. A most popular method is fuzzy c-means (Baumgartner et al., 1997, 1998; Moser et al., 1997; Golay et al., 1998; Moser et al., 1999). The standard K-means algorithm has also been used successfully (Ding et al., 1994; Toft et al., 1997; Goutte et al., 1999), including hierarchical approaches to clustering (Goutte et al., 1999; Filzmoser et al., 1999). Also, innovative methods using hierarchical arguments with a nonparametric approach are starting to appear (e.g., Wismu¨ ller et al., 1998; Domany, 1999; Goutte, unpublished research).

2. Introduction to Alzheimer's Disease

Alzheimer's disease (AD) is a chronic neurodegenerative disease that starts slowly and gradually gets worse over time. It is the main cause of cases of dementia. The most common early symptom is starting to forget about recent events. With the disease advances, symptoms can include language barrier, disorientation (including easily getting lost), mood swings, loss of motivation, not managing self-care, and behavioral issues. The Alzheimer's disease causes a person's condition declines, and they often withdraw from family and society. Gradually, the patients lose bodily functions, ultimately leading to death. Although the speed of progression can vary according to the patient, the typical life expectancy after the diagnosis is three to nine years.

The cause of Alzheimer's disease is quite uncertain. About 70% of the risk may be inherited from a person's parents, with related to genes. Other risk factors may include a history of head injuries, depression, and hypertension. The disease is associated with plaques and neurofibrillary tangles in the brain. A probable diagnosis is based on the history of illness and cognitive tests. Initial symptoms of Alzheimer's disease are often mistaken for normal ageing. Examination of

brain tissue is necessary for a definite diagnosis. The risk of AD may be reduced by mental and physical exercises. However, there is no strong evidence supporting this idea. Also, there are no medications that have been shown to decrease risk.

No treatments can stop or reverse its progression, though some may improve symptoms temporarily. Affected patients increasingly rely on others for assistance, often placing a burden on the one who take care of them. The pressures are from social, psychological, physical, and economic elements. Physical and mental exercise programs may be beneficial and can potentially improve symptoms. Behavioral problems due to dementia are often treated with antipsychotics, but this is not usually effective, as there is little improvement in symptoms and an increased risk of early death.

In 2015, there were about 29.8 million people worldwide affected with AD. It begins mostly in people over 65 years of age, although 4–5% of cases are early-onset Alzheimer's. About 6% of people older than 65 years old are affected by AD. In 2015, dementia resulted in about 1.9 million deaths worldwide. AD was first described by, and named after, German psychiatrist and pathologist Alois Alzheimer in 1906. AD is one of the most financially cost diseases in many developed countries.

3. Introduction to Cognitive Normal Elderly

Cognitive change with the normal process of aging has been well documented in the scientific literature. Some cognitive abilities, such as vocabulary, are resilient to aging and may even improve with age. Other abilities, such as conceptual reasoning, memory, and processing speed, decline gradually when a person gets elderly. There is significant difference among older adults in

the rate of decline in some abilities, such as perceptual reasoning and processing speed.

4. K-means Algorithm

Let $X = \{x_i\}, i = 1,...,n$ be the set of n-dimensional points. Cluster it into a set of K clusters, $C = \{c_k, k = 1,..., K\}$. The K-means algorithm is to segment all the points so that the squared error between the empirical mean of a cluster and the points in the cluster is minimized. Define μ_k as the mean of cluster c_k. The squared error between μ_k and the points in cluster c_k is calculated as

$$J(c_k) = \sum_{x_i \in c_k} \| x_i - \mu_k \|^2$$

The aim of K-means algorithm is to minimize the sum of the squared error in K clusters,

$$J(C) = \sum_{k=1}^{K} \sum_{x_i \in c_k} \| x_i - \mu_k \|^2$$

Minimizing this function is an NP-hard problem (even for K = 2) (Drineas et al., 1999). So K-means is a greedy algorithm. It can only converge to a local minimum, even though a study has shown with a large probability K-means could converge to the global optimum when clusters are separated well (Meila, 2006). K-means starts to generate K clusters and assign patterns to clusters in order to reduce the squared error. Since the squared error always when the number of clusters K increases (with J(C) = 0 when K = n), it should be minimized only for a fixed number of clusters. The main steps of the K-means algorithm are listed as follows (Jain and Dubes, 1988):

1. Put all the points in K clusters; repeat steps 2 and 3 until K clusters stabilizes.

2. Generate a new partition by assigning patterns to its closest cluster center.

3. Calculate new cluster centers.

5. Markov Chains

A Markov chain is a mathematical system that has transitions from one state to another. The transitions can be marked with its own probability. The characteristic of a Markov chain is that no matter how the process arrived at its present state, the future states are fixed. In other words, the probability of transitioning to any particular state is dependent on the current state and time. The states defined can be anything according to our needs, including letters, numbers, weather conditions and so on.

The changes of states in the system are called transitions. The probabilities associated with the state changes are called transition probabilities. The process is characterized by a state space, a transition matrix describing transition probabilities, and an initial state (or initial distribution) across the state space. We can assume that all possible states and transitions are included in the definition of the process, so there is always a next state, and the process of state changes does not terminate.

6. Sliding window PCA

The sliding window PCA is based on principle component analysis (PCA). In this method, a window is defined as a set of fMRI data of N_{vox} brain voxels within a range of time, N_{win} . A sliding window is defined to be the window shifted by N_{hop} timepoints from the beginning of the previous window. (Khairi et al., 2019) MATLAB is used to apply this method because it is based on matrix calculation. In the experiment, N_{win} is chosen as 20 and N_{hop} is chosen as 4. Thus, the first window is from timepoint 1 to timepoint 20, and the second window is from timepoint 5 to

timepoint 24.

A. The Proposed Method

Let X be the whole-brain fMRI data with T timepoints and N voxels. In MATLAB, X is a $T \times N$ matrix. The cross-correlation of all the voxels with size of $T \times T$ can be calculated as

$$R = XX^T$$

Let I be a diagonal matrix with ones on the diagonal with size of $N_{win} \times N_{win}$. Then, let $\tilde{I}_t$ be an $T \times T$ matrix with zeros except at row t to $t+(N_{win}-1)$ and column t to $t+(N_{win}-1)$ which is replaced with matrix I .

$$I = \begin{bmatrix} 1 & 0 & 0 \\ 0 & \ddots & 0 \\ 0 & 0 & 1 \end{bmatrix}$$

$$\tilde{I}_t = \begin{bmatrix} 0 & 0 & 0 & 0 \\ 0 & I & 0 & 0 \\ 0 & 0 & 0 & 0 \\ 0 & 0 & 0 & 0 \end{bmatrix}$$

The target of sliding window PCA is to calculate the components c_i and observe their changes in each window. The components generated by PCA explains the variance in the fMRI data between AD and CN subjects because the dimensionality of dataset is reduced. The defined components can be more reliable to see the brain activities from one window to another. The principle components point in the direction of maximum variation and indicate the set of times over which maximum changes occurs. For the first component values for each timepoint, c_1 is obtained from first column of the left singular vectors of the normal singular value decomposition

(SVD) method. This will result in c_1 as a vector size of $T \times 1$. For the subsequent component values, we want to choose the $c_i I_t c_{i+1}$ to be as minimum as possible to ensure the components to be as orthogonal as possible.

If we use PCA strictly, the orthogonality rules require that $c_i^T c_{i+1}$ has to be equal to 1 and thus forcing $c_i I_t c_{i+1}$ to be zero. Our method is designed to loosen the constraint to at least a minimum instead of strictly orthogonal as in PCA.

B. Maximization of Subsequent Components Fractions

To obtain the subsequent components, we need to maximize

$$\frac{c_i{}^T R c_i}{c_i{}^T (D^T D) c_i}$$

where

$$D = \begin{bmatrix} c_{i-1}^T I_1 \\ c_{i-1}^T I_2 \\ \vdots \\ c_{i-1}^T I_n \end{bmatrix}$$

and n is the total number of windows.

This can be done by minimizing the denominator $c_i^T (D^T D) c_i$ through restricting the component i .

The whole algorithm is summarized in Algorithm 1. As the final outcome, each window will have a set of basis vectors. For example, a set of data containing 1200 timepoints and processed

with sliding-window configuration of N_{win} and N_{hop} of 20 and 4 respectively will have five basis vectors of length 1200.

Algorithm 1 Ratio Maximization

1: $R = XX^T$

2: $c_1 \leftarrow$ First component from PCA(R) (In MATLAB, it is calculated as[U1,~,~]=svd(R); c1 = U1(:,1);)

3: **for** each subsequent component i, c_i **do**

4: **for** each window j **do**

5: Create $\tilde{I}_t$

6: **end for**

7: Create D

8: Find c_i that minimizes $c_i^T (D^T D) c_i$

9: **end for**

Chapter II. Methods

1. Data Collection

The source of data is from the database of Alzheimer's Disease Neuroimaging Initiative (ADNI), which is called Image and Data Archive (IDA, https://ida.loni.usc.edu/). Raw MRI data of different subjects can be found in the IDA. To get the exact type of raw data we need, in advanced search (beta), research group is chosen as Alzheimer's disease (AD) and cognitive normal (CN), and modality as fMRI. Then 17 Alzheimer's disease (AD) and 12 cognitive normal (CN) subjects are randomly chosen from a variety of ages, so that the results and conclusions can be robust enough for difference between Alzheimer's disease (AD) and cognitive normal (CN) subjects. The last step is adding them to data collections and downloading them as NIFTI files, including fMRI data and Magnetization Prepared - RApid Gradient Echo (MPRAGE, T1-weighted) data.

For all the fMRI data, the field strength is 3.0 tesla, the resolution is 64x64x48, the TR is 3000.0 ms, the slice thickness is 3.3ms or 3.4ms, the manufacturer is Philip Medical systems or SIEMENS. For all the MPRAGE data, the acquisition plane is SAGITTAL, the field strength is 3.0 tesla, the manufacturer is Philip Medical systems or SIEMENS, the slice thickness is 1.0mm or 1.2 mm, the resolution is different for all the subjects, and a typical one is 256x256x211. And for all the subjects, the number of timepoints is 140 or 197.

A major advantage of using thicker slices is that the time to scan a given brain volume is inversely proportional to the slice thickness used (Howseman et al., 1999). On the other hand, brain areas most affected by magnetic susceptibility artifacts will be less susceptible to signal

dropout problems if imaged using thinner slices. Furthermore there is some evidence that the use of small gaps between the imaging slices may help to reduce the extreme sensitivity of functional MRI to stimulus-correlated motion.

2. Preprocessing of Raw Data

For the convenience of the following analysis, the data need to be transformed to the same space. I use FMRIB Software Library (FSL) to do the preprocessing of the fMRI data from the lower dimensional space to the standard MNI (Montreal Neurological Institute) space (91x109x91) as well as the alignment. First, I run Brain Extraction Tool (BET) on the raw MPRAGE files to get the brain-extracted MPRAGE image and the binary brain mask image. BET deletes non-brain tissue from an image of the whole head. The main parameters I adjust in BET is fractional intensity threshold and threshold gradient. The larger the fractional intensity threshold is, the smaller the brain outline is. The negative threshold gradient can give smaller brain outline at bottom. Then, I run FMRIB's Automated Segmentation Tool (FAST) segmentation on the brain-extracted MPRAGE image. FAST segments a 3D image of the brain into different tissue types (Grey Matter, White Matter, CSF, etc.). Note that I click on “Binary segmentation: Also output one image per class”. There should be four outcome files. The one we need is seg_1, which is the gray matter mask, and seg_2, which is the white matter mask. FMRIB's Linear Image Registration Tool (Flirt) can be used to transform the mask files to the MNI space. FLIRT is a fully automated robust and accurate tool for linear (affine) intra- and inter-modal brain image registration. The reference image I choose is MNI152_T1_2mm_brain_mask. Finally, I do the registration on the fMRI data. Before that, I have transformed all the fMRI data to a 4d one in each subject. Steps and codes are listed as following.

1. **EPI TO T1_brain** (output: trans matrix for EPI to T1brain)

flirt -in fMRI.nii -ref MPRAGE_brain.nii -dof 12 -omat func2struct.mat

2. **T1_brain to MNI** (output: T12MNI.nii & trans matrix for T1brain to MNI)

flirt -in MPRAGE_brain.nii.gz -ref /usr/local/fsl/data/standard/MNI152_T1_2mm_brain -omat T1_to_MNI_affine.mat -bins 256 -cost mutualinfo -searchrx -90 90 -searchry -90 90 -searchrz -90 90 -dof 12 -out T12MNI.nii.gz

3. **T1 to MNI** (output: nonlineartrans matrix for T1 to MNI - additional matrix)

fnirt --in=MPRAGE.nii --aff=T1_to_MNI_affine.mat --cout=nonlinear_trans --config=T1_2_MNI152_2mm

4. **EPI to MNI** (output: EPI2MNI.nii)

applywarp --in=fMRI.nii --ref=/usr/local/fsl/data/standard/MNI152_T1_2mm_brain --warp=nonlinear_trans --premat=func2struct.mat --out=EPI2MNI

Then, spatial filter and temporal filter is applied to get xcell and xcellmask. Each voxel time series was filtered using a finite impulse response (FIR) bandpass filter with TR=3.

3. Data Analysis

The Instantaneous Whole Brain Correlation (IWBC) of each subject is computed and figured (Bell, 2018). At each of the time points, a whole brain correlation (WBC) for a single time point

is performed. The instantaneous WBCs for a single time point t were calculated according to following equation:

$$WBC_t = \frac{1}{2}\sum^{i}\sum^{j}\frac{1}{n}\frac{(x_i - \overline{x_i})(y_j - \overline{y_j})}{\sigma_{x,i}\sigma_{y,j}}$$

where x and y are voxels, and i and j iterate over v voxels for $i \neq j$. The entry i and j indicates how similar the brain activity is at times i and j.

Feature matrix characterized by activation level of six rough brain regions is computed. The feature matrix includes the number of active voxels in it. Then, feature matrix characterized by activation level of Brodmann areas (von Economo, 1925) are computed, including frontal lobe, parietal lobe, temporal lobe, occipital lobe and cingulate cortex. K-means clustering characterized by rough brain regions and Brodmann areas is performed. All the time points are classified into K clusters. The K-means clustering results show the average number of active voxels in the featured regions. The results are used to perform Markov chains and CAP analysis to find differences in the brain activity patterns between AD and CN subjects. The K-means algorithm iterates the following steps:

1. Initialize K clusters C_k , $k = 1,...,K$, with centers $c_k^{(i)}$, for iteration $i = 0$.

2. Assign each data vector u_j to the cluster C_k with the nearest center $c_k^{(i)}$, based on a distance metric between the cluster center and the data vector $d(u_j, c_k^{(i)})$.

3. Set new cluster center $c_k^{(i+1)}$ to the average of its members: $c_k^{(i+1)} = \frac{1}{|C_k|}\sum_{j \in C_k} u_j$.

Then, a Markov chain model (Metropolis, 1953) is estimated and plotted. The Markov chain shows the exact transition probabilities for time points in K clusters that transit to next time point. From the Markov chain, different patterns of AD and CN can be found. Spatial and temporal co-activation pattern (CAP) is figured (Liu et al., 2018). Temporal CAP shows the classification of states on IWBC for each time point. Spatial CAP shows the average number of active voxels in Major resting-state networks (RSNs) (Doucet et al., 2018), including default-mode (DMN), central executive (CEN), salience (SAL), visual (VIS), and sensorimotor (SMN) networks. Sliding window Principle Component Analysis (PCA) is applied to provide some insight on the changes in the fMRI data where there could be the possibility of brain synchronizing when most of the brain regions are highly correlated. The values of five transform coefficient are displayed in the results.

Chapter III. Results

1. Preprocessing

Preprocessing is done on all the 17 AD and 12 CN subjects. Figure 1 shows an original structural MRI image. Figure 2 shows the structural MRI image in MNI space with the skull removed.

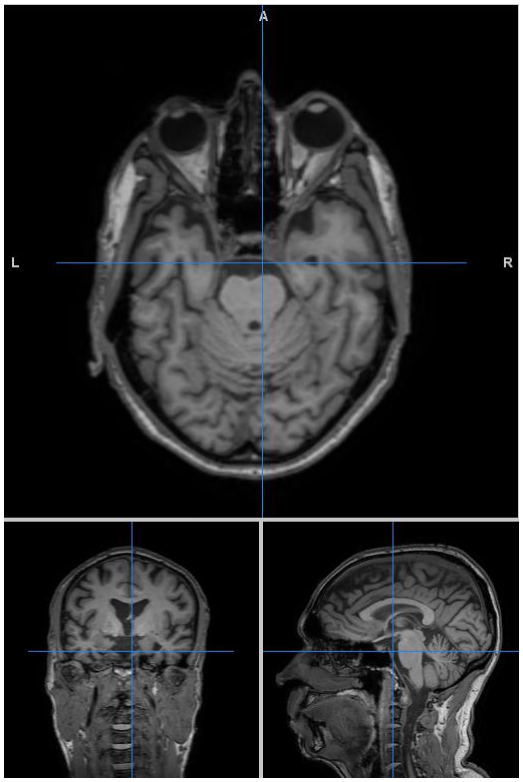

Figure 1 Original structural MRI image of AD subject 006_S_4153

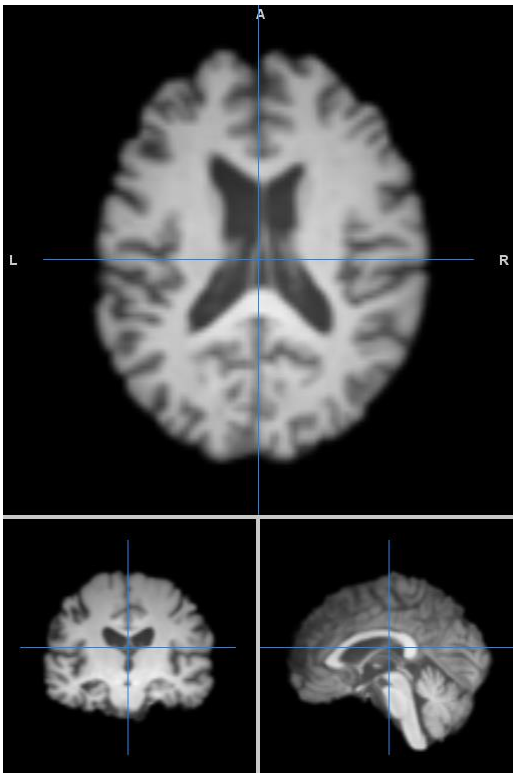

Figure 2 Skull-removed structural MRI image of AD subject 006_S_4153 in MNI space

2. Clustering

K-means clustering is done in Brodmann areas within major brain lobes, including frontal lobe, parietal lobe, temporal lobe, occipital lobe and cingulate cortex, for all the AD and CN subjects. Different k values are tried. Figure 3 and Figure 4 show the clustering results for AD subject 002_S_5018 when k is 10 and 6, respectively. In each case the numbers of active voxels in each lobe and Brodmann area are counted.

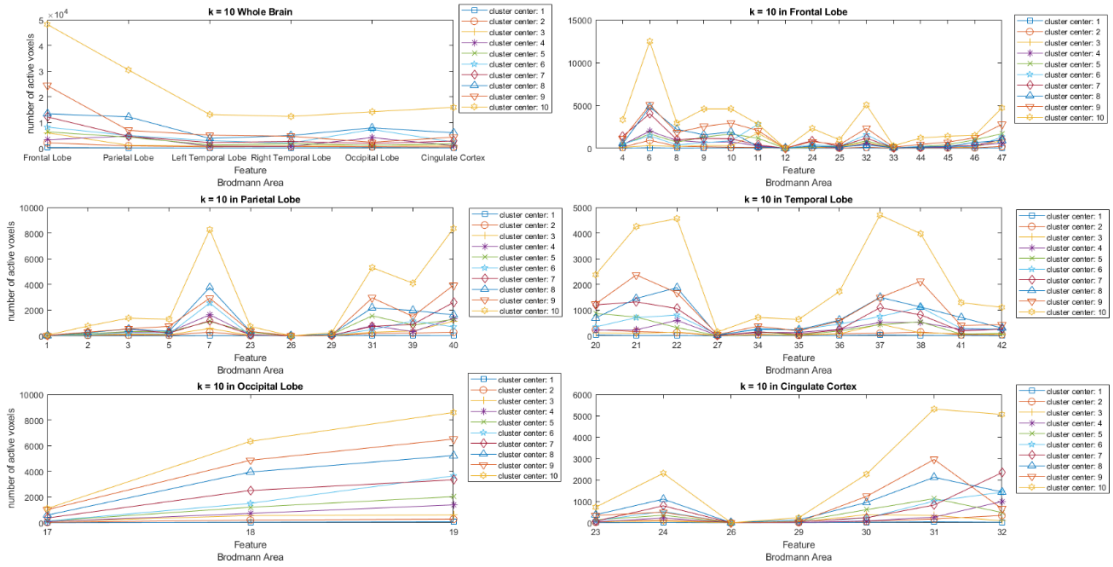

Figure 3 Clustering result of AD subject 002_S_5018, k=10

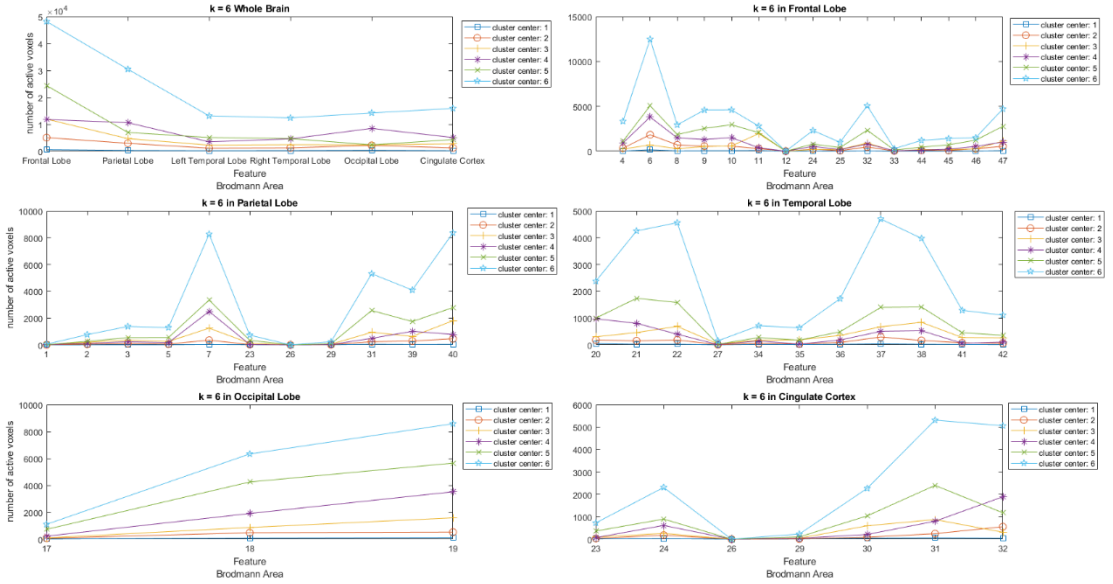

Figure 4 Clustering result of AD subject 002_S_5018, k=6

Figure 5 shows the clustering results of AD subject 003_S_6264 when k=10. Figure 6 shows the clustering results of CN subject 002_S_0295 when k=10. Figure 7 shows the clustering results of CN subject 002_S_0413 when k=10.

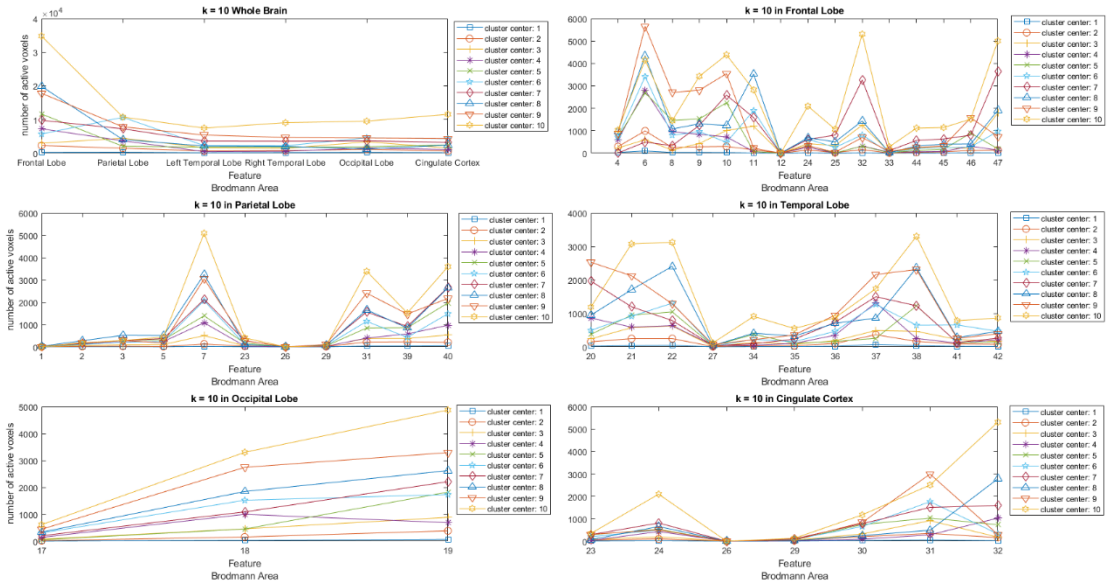

Figure 5 Clustering result of AD subject 003_S_6264, k=10

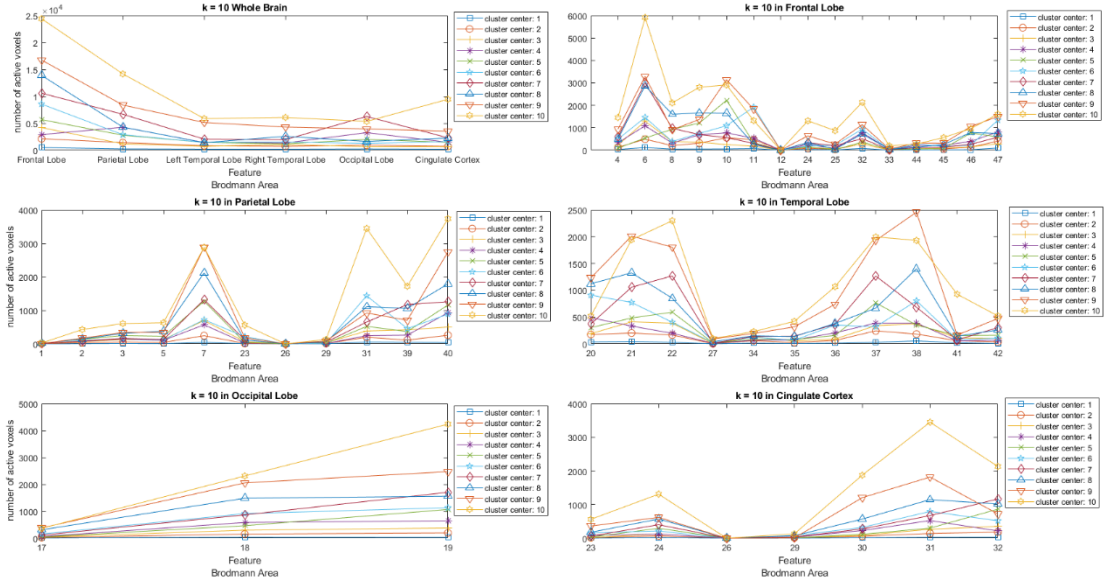

Figure 6 Clustering result of CN subject 002_S_0295, k=10

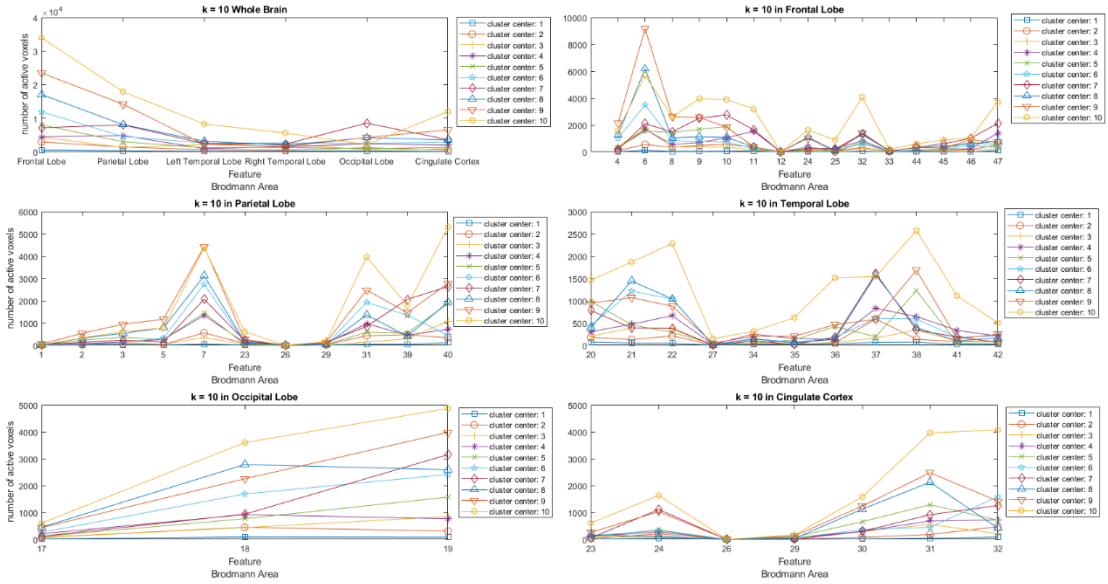

Figure 7 Clustering result of CN subject 002_S_0413, k=10

3. Markov Chain Model

Markov chain model is applied by estimating the probabilities of the state transitions. Figure 8 and Figure 9 are the Markov chain result of AD subject 002_S_5018 when k = 6 and 10.

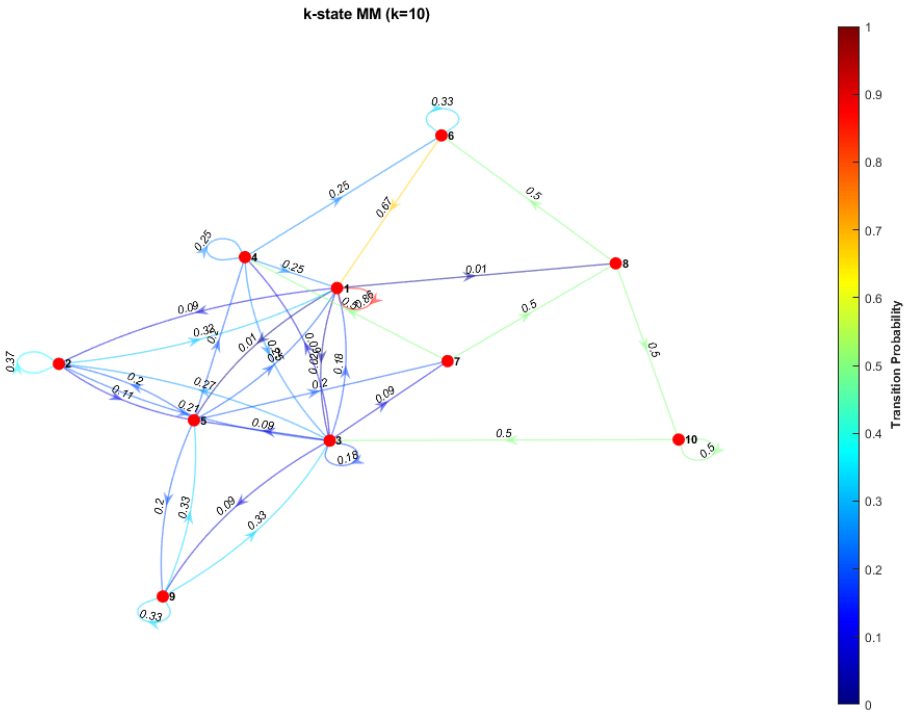

Figure 8 Markov chain result of AD subject 002_S_5018, k=10

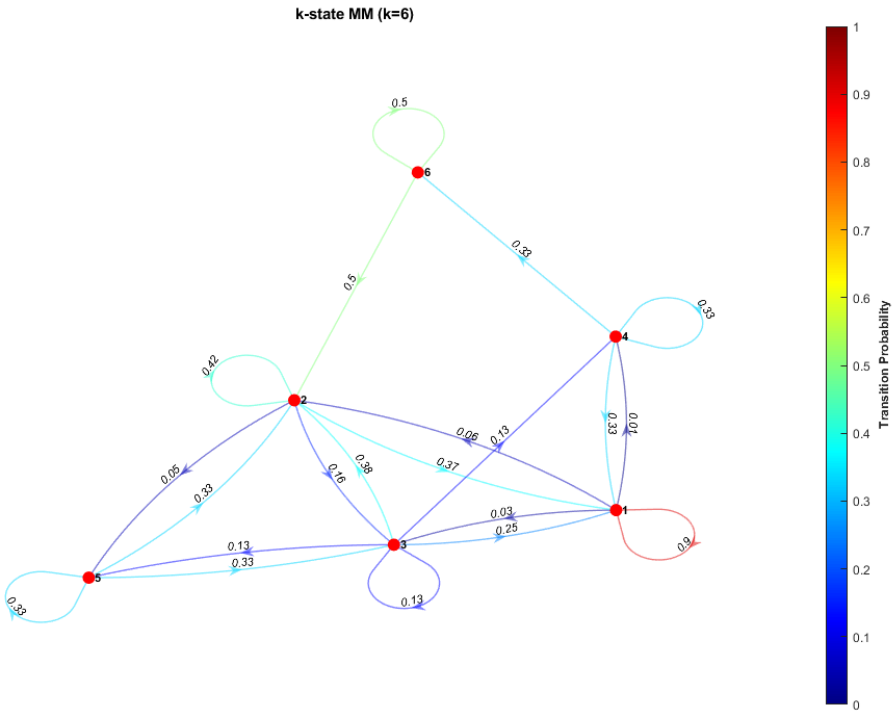

Figure 9 Markov chain result of AD subject 002_S_5018, k=6

Figure 10 shows the Markov chain of CN subject 002_S_0295 when k=10. Figure 11 shows the Markov chain of CN subject 002_S_0413 when k=10.

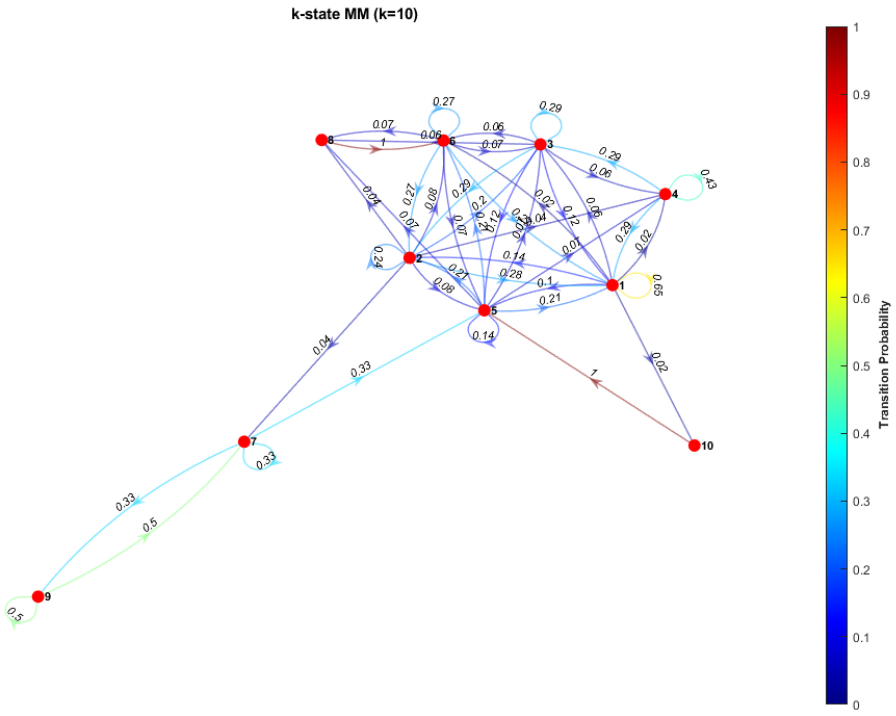

Figure 10 Markov chain result of CN subject 002_S_0295, k=10

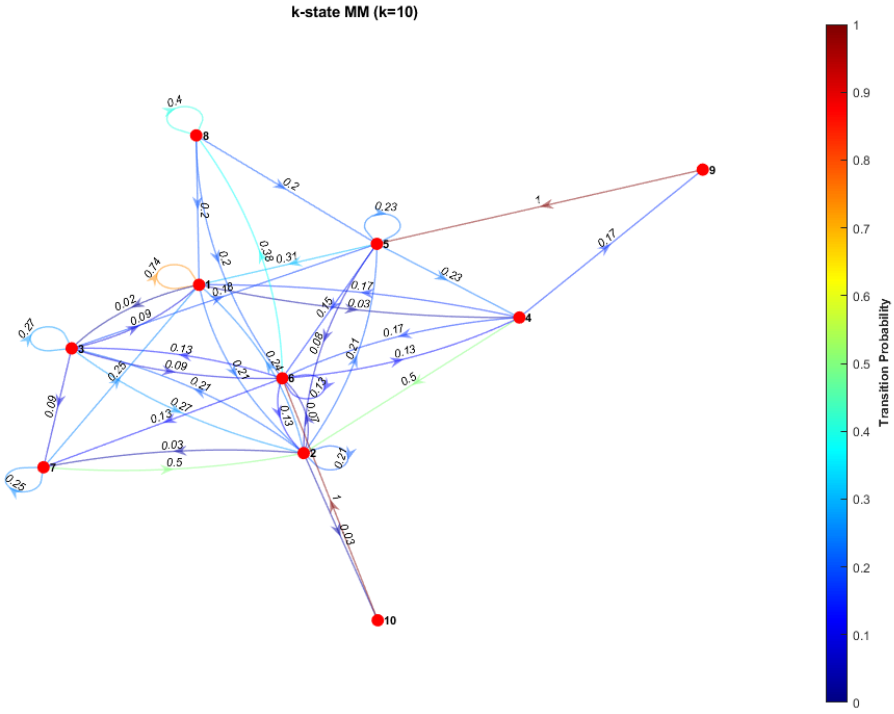

Figure 11 Markov chain result of CN subject 002_S_0413, k=10

4. CAP Analysis

The CAP analysis consists of two parts, spatial CAP and temporal CAP. In the spatial CAP, we can observe the changes of clusters in Major resting-state networks (RSNs) (Doucet et al., 2018), including default-mode (DMN), central executive (CEN), salience (SAL), visual (VIS), and sensorimotor (SMN) networks. In temporal CAP, we can observe the IWBC with the states marked on it. Figure 12 and Figure 13 show the spatial CAP and temporal CAP of AD subject 002_S_5018 when k=10.

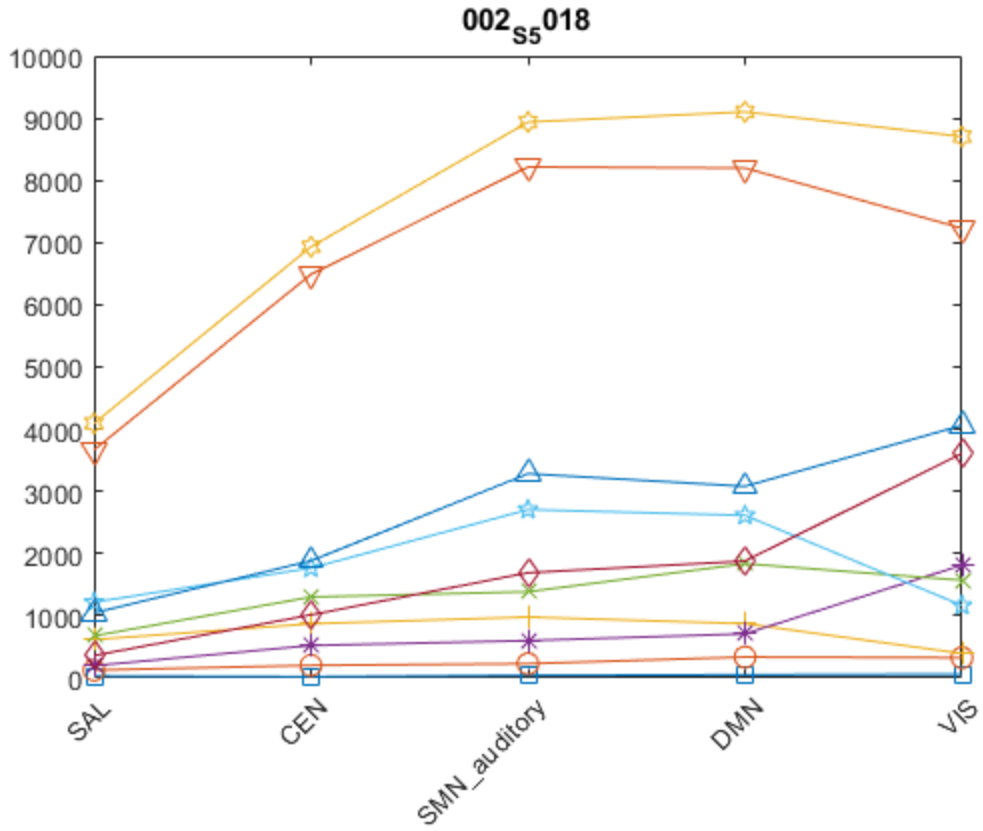

Figure 12 Spatial CAP result of AD subject 002_S_5018, k=10

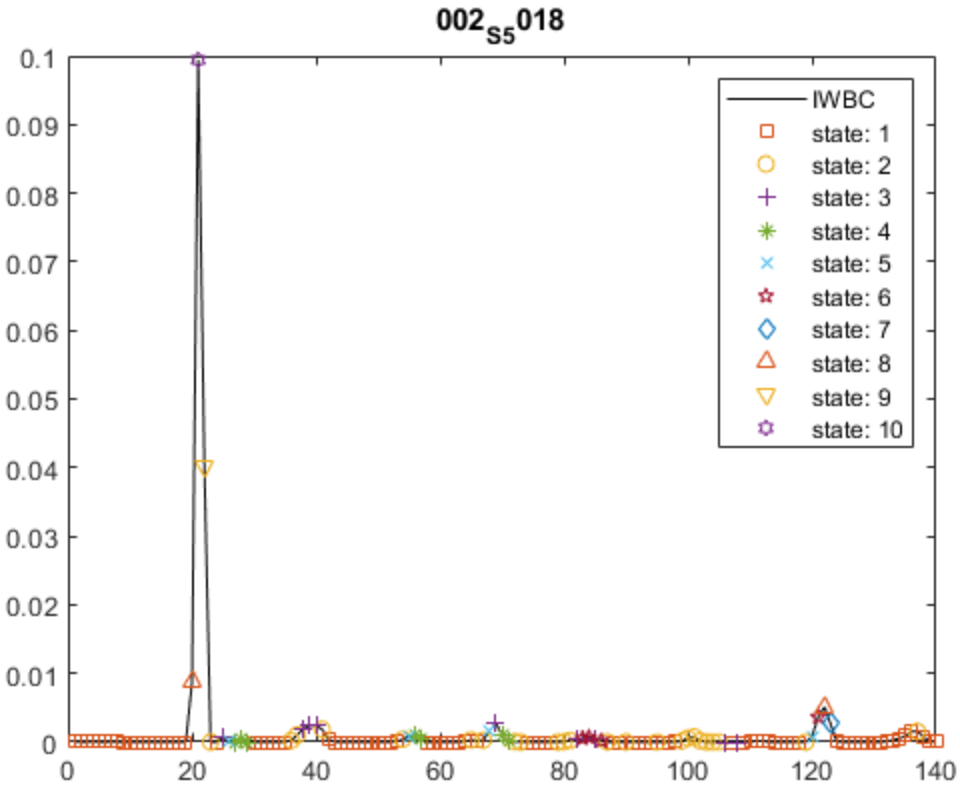

Figure 13 Temporal CAP result of AD subject 002_S_5018, k=10

Figure 14 and Figure 15 shows the spatial CAP and temporal CAP of AD subject 003_S_6264 when k=10.

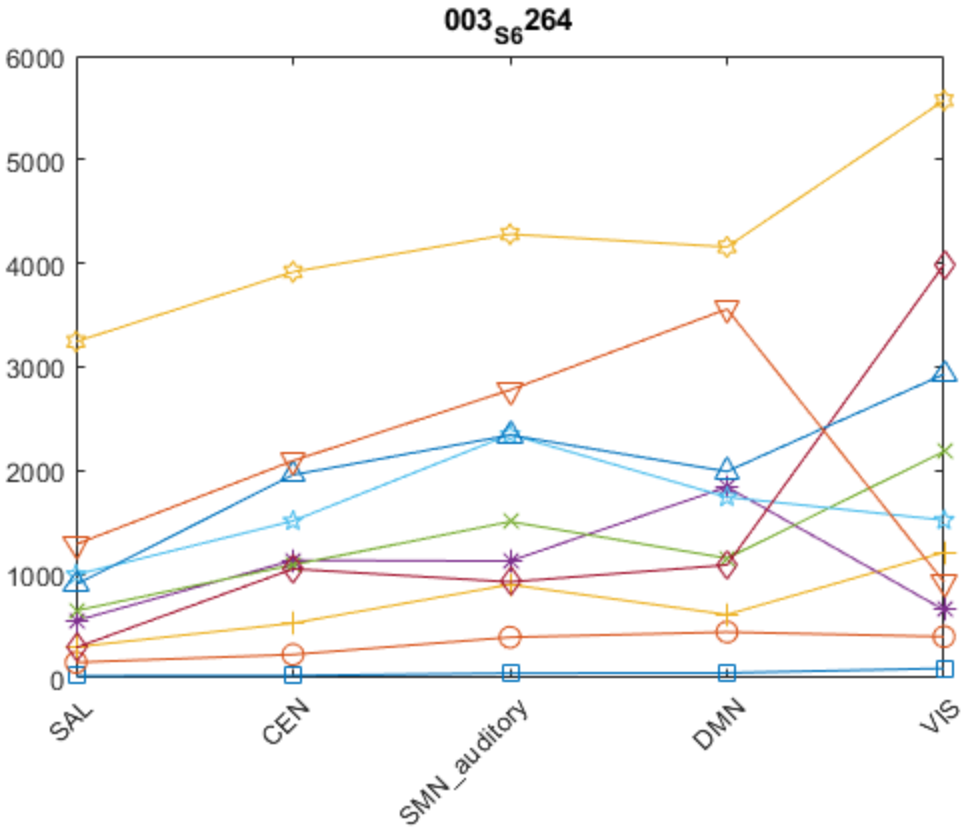

Figure 14 Spatial CAP result of AD subject 003_S_6264, k=10

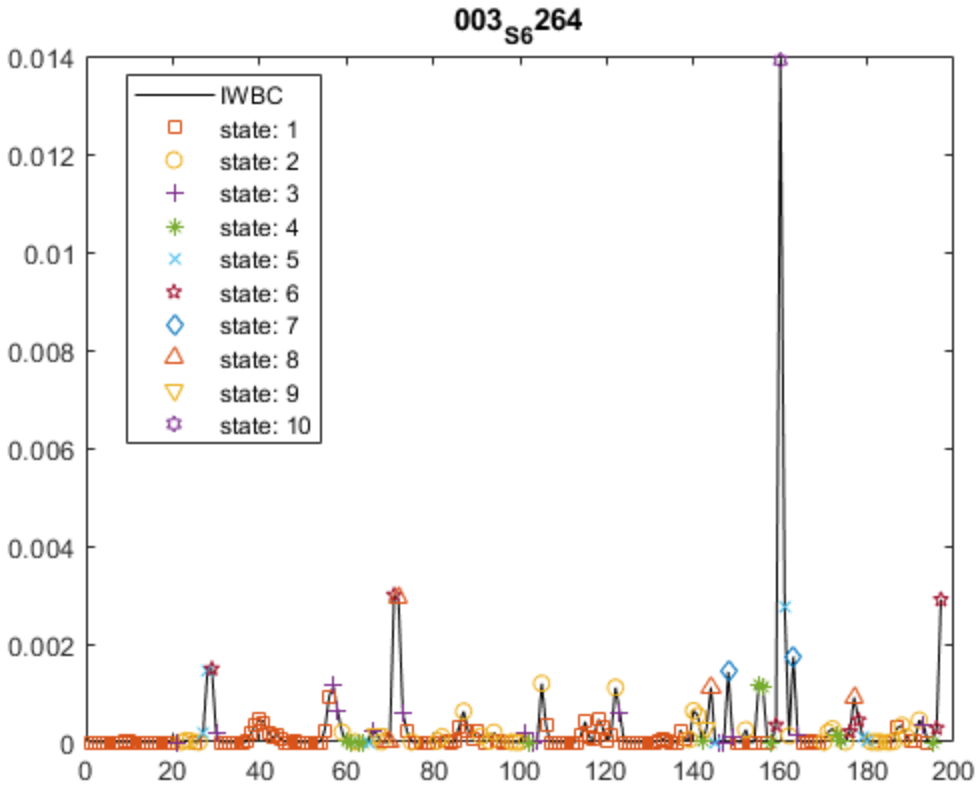

Figure 15 Temporal CAP result of AD subject 003_S_6264, k=10

Figure 16 and Figure 17 shows the spatial CAP and temporal CAP of CN subject 002_S_0295 when k=10.

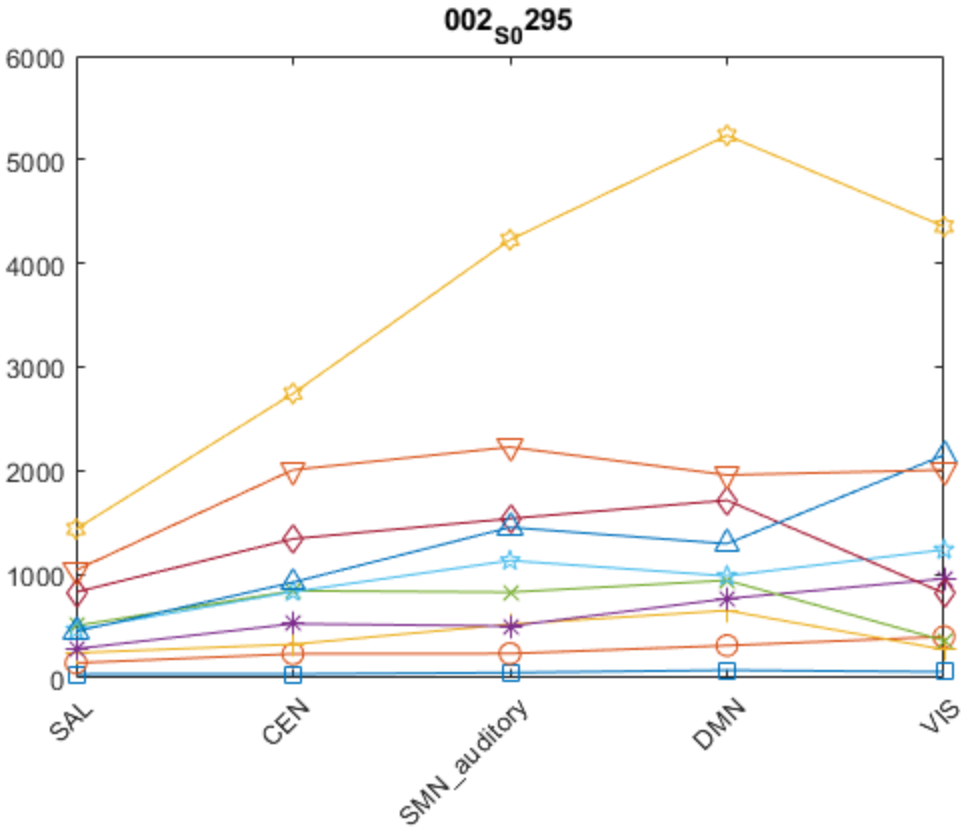

Figure 16 Spatial CAP result of CN subject 002_S_0295, k=10

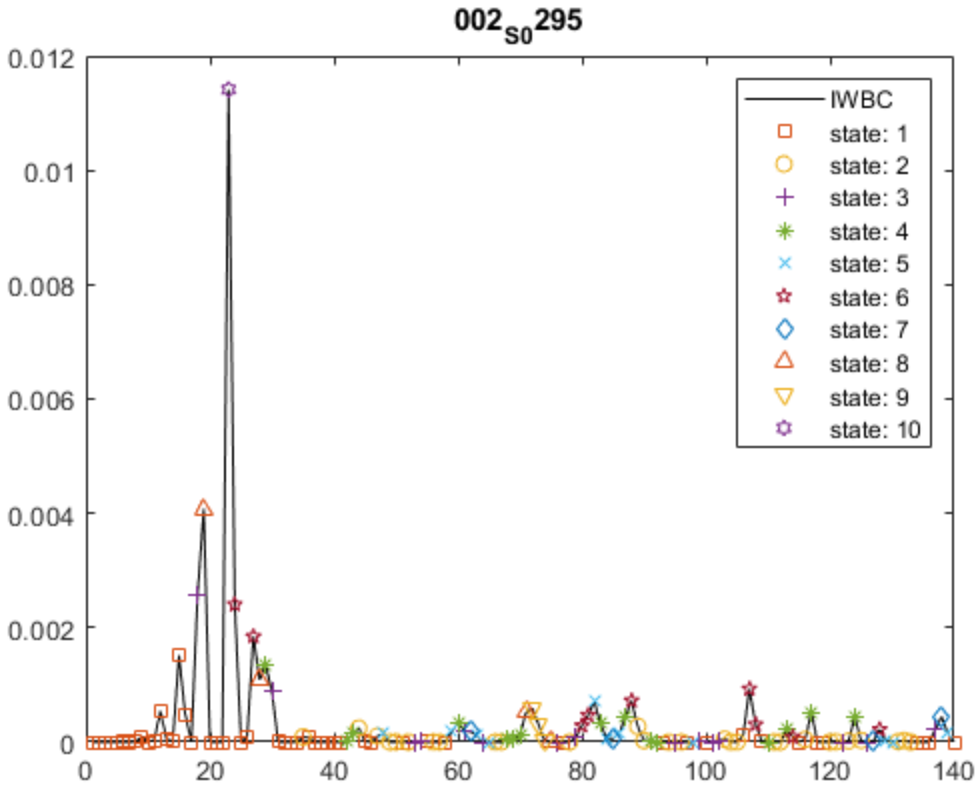

Figure 17 Temporal CAP result of CN subject 002_S_0295, k=10

5. Sliding Window PCA

According to the sliding window algorithm, the Nwin I use is 20, the Nhop is 4. Win 1 includes timepoint 1 to 20. Win 2 includes timepoint 5 to 24, etc. Figure 18 shows the timescore of AD subject 130_S_4982.

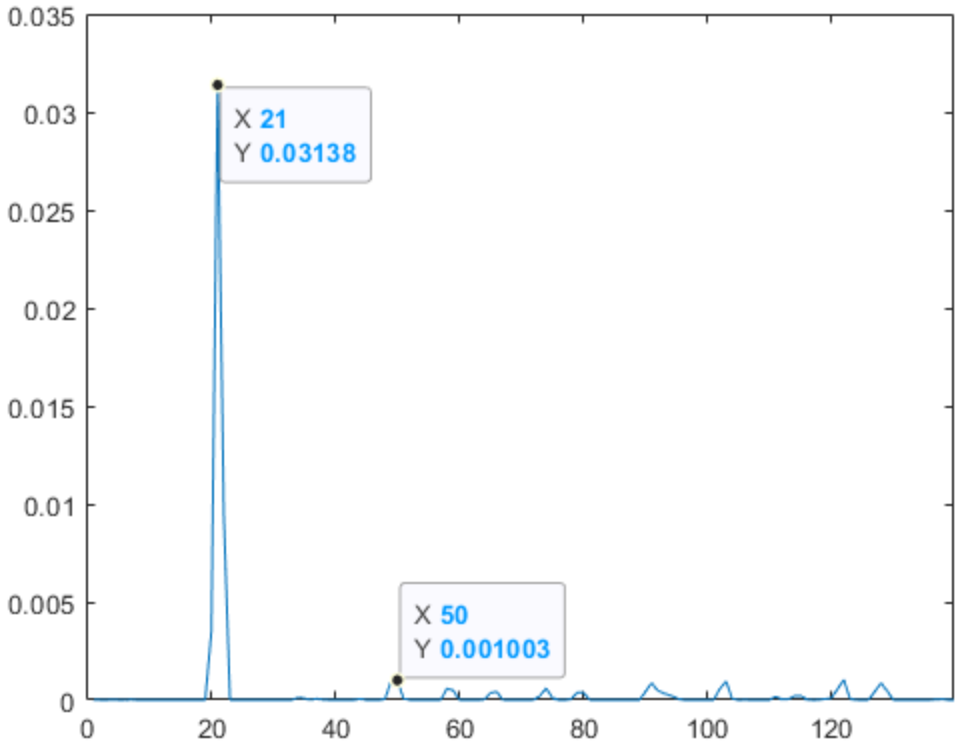

Figure 18 IWBC of AD subject 130_S_4982

From the IWBC, we can capture the two large peaks at timepoint 21 and timepoint 50. So we do sliding window PCA around these two timepoints. Figure 19 shows the sliding window results for timepoint 21. Figure 20 shows the sliding window results for timepoint 50.

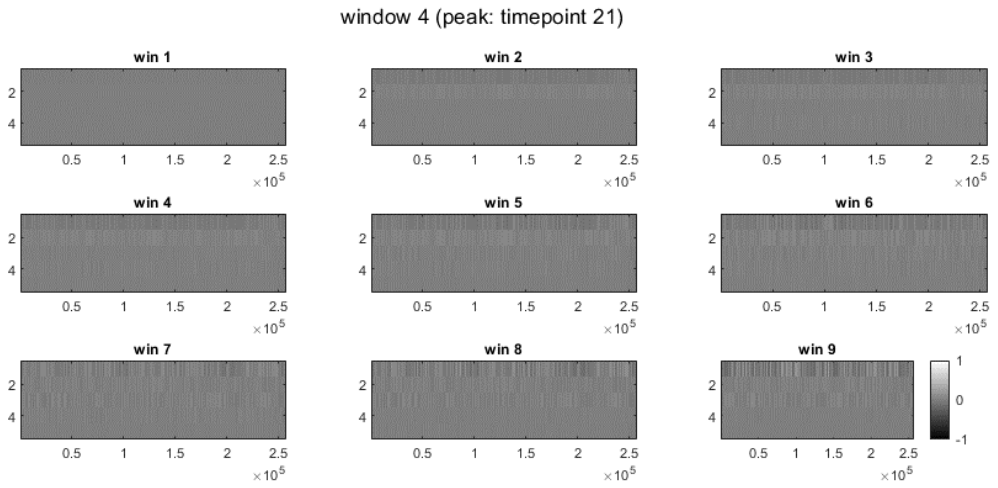

Figure 19 Sliding window result of AD subject 130_S_4982 for timepoint 21

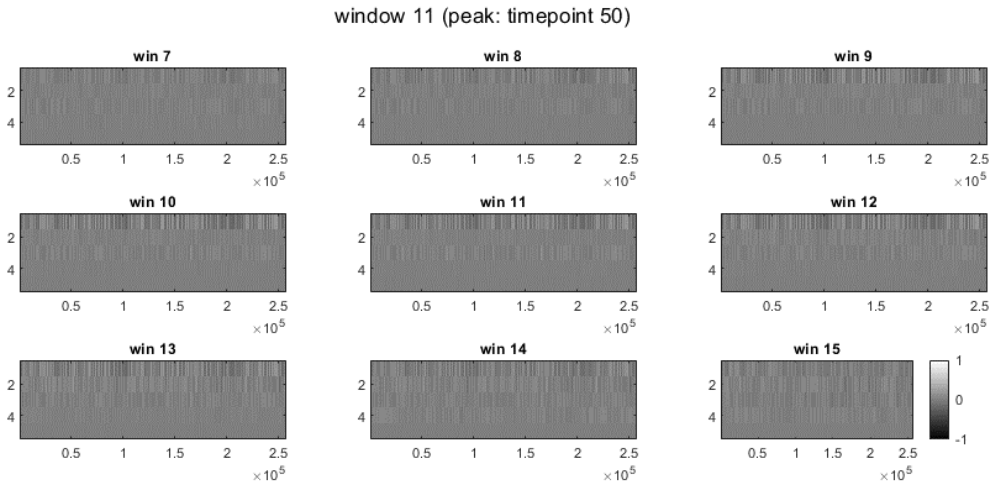

Figure 20 Sliding window result of AD subject 130_S_4982 for timepoint 50

Similarly, the sliding window PCA is applied on CN subject 037_S_0303. Figure 21 shows the IWBC for it.

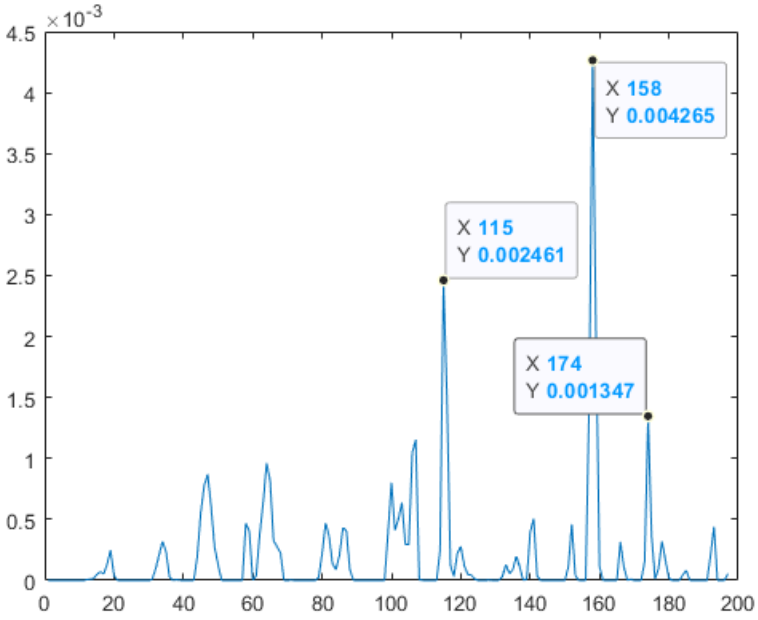

Figure 21 IWBC of CN subject 037_S_0303

Figures 22, 23 and 24 shows the sliding window results of CN subject 037_S_0303 for its three peak timepoints 115, 158 and 174.

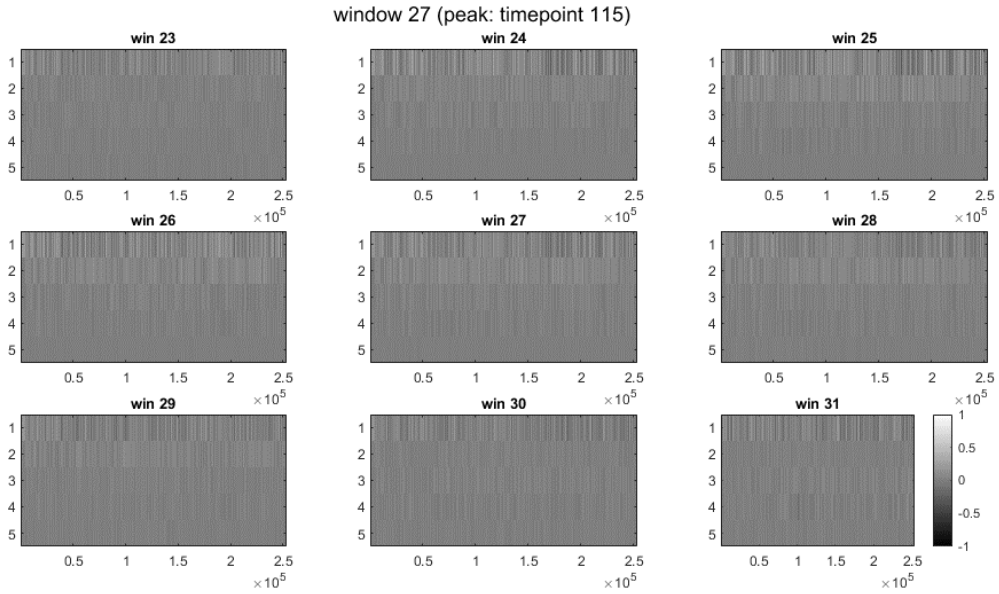

Figure 22 Sliding window result of CN subject 037_S_0303 for timepoint 115

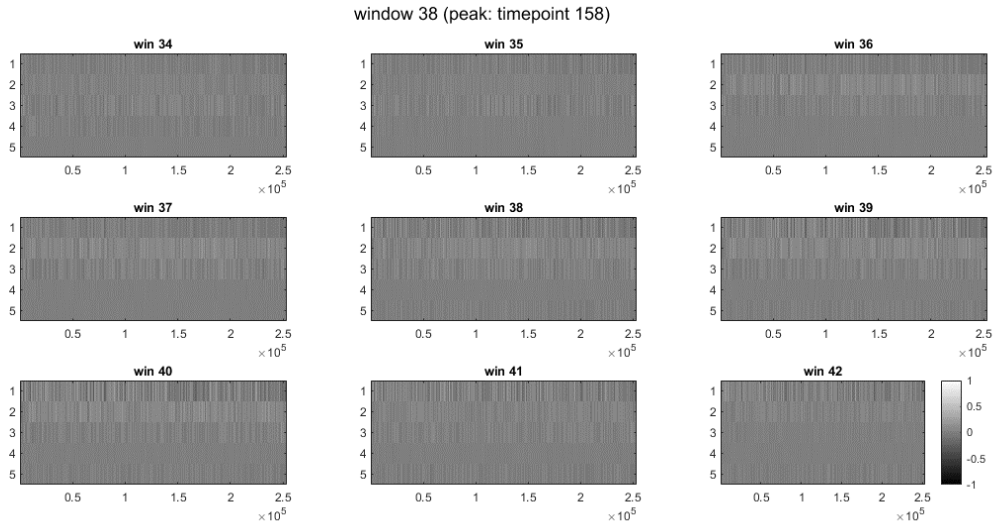

Figure 23 Sliding window result of CN subject 037_S_0303 for timepoint 158

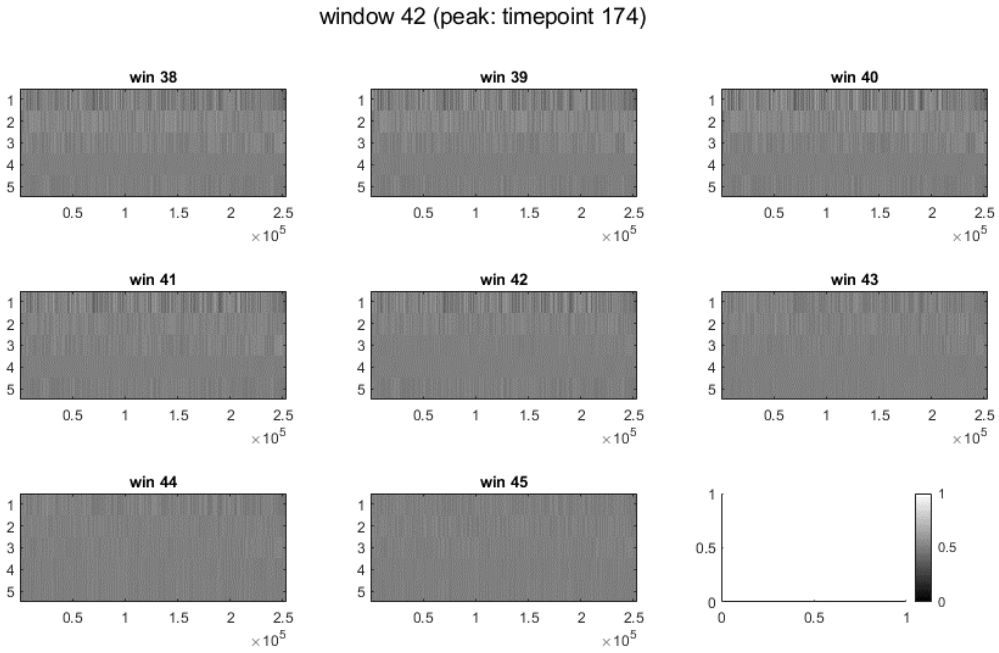

Figure 24 Sliding window result of CN subject 037_S_0303 for timepoint 174

Chapter IV. Discussion

1. Clustering

From Figure 3 and Figure 4, different k values may have a similar pattern of clustering results. When k is greater, it is more easily to see lines of different clusters intersecting with each other. From Figure 3, 5 ,6 and 7, by contrasting the clustering results of AD and CN subjects with the same k value, it can be seen that the frontal lobe is always the most active part of the whole brain, then the parietal lobe. Also, in AD subjects, the left temporal lobe, the right temporal lobe, the occipital lobe and the cingulate cortex are smoother than they are in CN subjects. Actually, the occipital lobe and the cingulate cortex have more crossing lines in AD subjects, which can be seen from the whole brain part. It reveals that the occipital lobe and the cingulate cortex are more active in AD subjects than they are in CN subjects.

2. Markov Chain Model

From Figure 8 and Figure 9, different k values may have a similar pattern of clustering results. From Figures 8, 10 and 11, when the k value is the same, some similarity and different points can be obtained from the Markov chain model results in AD and CN subjects. First, the state one always has a high probability when the transition is to itself. Second, we can separate the Markov chain model results in two parts, a part with many states densely connecting with each other, and a part for some states that only transition to one or two specified states. For example, in Figure 10, states 10, 9 and 7 is the second characteristic. And the rest of the states consist of the part

connecting densely to each other. In the CN subjects, the first part may have more connections in states, and the two-part pattern is more obvious in CN subjects than it is in AD ones.

3. CAP Analysis

From Figures 12, 14 and 16, in spatial CAP results, the VIS is more active in AD subjects than it is in CN ones. From Figure 10 and Figure 17, when combining the results of the Markov chain model and the IWBC, it can be observed that most points in state one are on the horizontal line of zero, and most points that have a value of nearly zero are in state one. So it explains why state one has a high probability when the transition is to itself. Additionally, the highest peak is in state 10, the second highest one is in state 8, which shows large peaks are more likely to be in the last several states.

4. Sliding Window PCA

From Figure 19, the peak timepoint 21 is in window 2 to window 6. The five transform coefficients may have some kind of changes when the peak point is in the window. And from Figure 20, the peak timepoint 50 is in window 9 to window 13. By contrasting window 8 and window 9, it can be seen that when the peak point enters a window, this window may have a greater change in the five transform coefficients than the former window. This can also be noticed in Figures 22, 23 and 24. Also, after the peak point leaves the window, the window may have a tendency to have a slighter change on the five transform coefficients. Future work can be done to explore those changes of the transform coefficients.

Chapter V. Conclusions

In this thesis, we applied several data analysis methods on fMRI data to detect the different patterns in brain activation levels between AD and CN patients. MPRAGE and fMRI raw data files of AD and CN subjects are downloaded from IDA. Preprocessing is done with FSL to remove the non-brain part in the raw fMRI and MPRAGE data. To investigate brain behavior during avalanches, a WBC was performed for each of the AD and CN subjects at each of time points at which the BOLD fMRI data was sampled. K-means clustering is performed by rough brain regions and Brodmann areas. The results reveal that different patterns of brain activation levels can be find between AD and CN patients, especially in the occipital lobe and the cingulate cortex. A Markov chain model (Metropolis, 1953) is estimated and plotted for each of AD and CN subjects. The Markov chain shows the exact transition probabilities for time points in K clusters that transit to next time point. From the Markov chain, different patterns of AD and CN can be found. CAP analysis is done for each of the AD and CN subjects. Spatial CAPs show that there may be some difference in RSNs for AD and CN subjects, exactly the VIS network. Temporal CAPs show they are consistent with IWBC magnitudes and Markov chain results. A sliding window PCA is applied to discover how five transform coefficients change in AD and CN subjects.

In conclusion, in-depth understanding of the structure and functionality of the brain is essential, from both a scientific and clinical standpoint. Pre-clinical Alzheimer's disease can be defined according to the differences in brain activities discovered in this work. Future work can be done based on the IWBC and more analysis can be applied, including head motion and phase transition to find more differences.

References

Bandettini, P. A., Jesmanowicz, A., Wong, E. C., & Hyde, J. S. (1993). Processing strategies for time-course data sets in functional MRI of the human brain. *Magnetic resonance in medicine*, *30*(2), 161-173.

Bassett, S. S., Yousem, D. M., Cristinzio, C., Kusevic, I., Yassa, M. A., Caffo, B. S., & Zeger, S. L. (2006). Familial risk for Alzheimer's disease alters fMRI activation patterns. *Brain*, *129*(5), 1229-1239.

Baumgartner, R., Scarth, G., Teichtmeister, C., Somorjai, R., & Moser, E. (1997). Fuzzy clustering of gradient-echo functional MRI in the human visual cortex. Part I: Reproducibility. *Journal of Magnetic Resonance Imaging*, *7*(6), 1094-1101.

Baumgartner, R., Windischberger, C., & Moser, E. (1998). Quantification in functional magnetic resonance imaging: fuzzy clustering vs. correlation analysis. *Magnetic Resonance Imaging*, *16*(2), 115-125.

Bell, C. S. (2018). *Seed-based correlation analysis and instantaneous global correlation analysis for resting state fMRI*. Vanderbilt University.

Ding, X., Tkach, J., Ruggieri, P., & Masaryk, T. (1994). Analysis of time-course functional MRI data with clustering method without use of reference signal. In *Proceedings of the International Society for Magnetic Resonance, 2nd Meeting, San Francisco, California* (Vol. 2, p. 630).

Domany, E. (1999). Superparamagnetic clustering of data-The definitive solution of an ill-posed problem. *Progress in Statistical Physics*, 213.

Doucet, G. E., Lee, W. H., & Frangou, S. (2019). Evaluation of the spatial variability in the major resting-state networks across human brain functional atlases. *Human brain mapping*, *40*(15), 4577-4587.

Drineas, P., Frieze, A., Kannan, R., Vempala, S., & Vinay, V. (2004). Clustering large graphs via the singular value decomposition. *Machine learning*, *56*(1-3), 9-33.

Eklund, A., Nichols, T. E., & Knutsson, H. (2016). Cluster failure: Why fMRI inferences for spatial extent have inflated false-positive rates. *Proceedings of the national academy of sciences*, *113*(28), 7900-7905.

Filzmoser, P., Baumgartner, R., & Moser, E. (1999). A hierarchical clustering method for analyzing functional MR images. *Magnetic resonance imaging*, *17*(6), 817-826.

Golay, X., Kollias, S., Stoll, G., Meier, D., Valavanis, A., & Boesiger, P. (1998). A new correlation-based fuzzy logic clustering algorithm for FMRI. *Magnetic Resonance in Medicine*, *40*(2), 249-260.

Goutte, C., Hansen, L. K., Liptrot, M. G., & Rostrup, E. (2001). Feature-space clustering for fMRI meta-analysis. *Human brain mapping*, *13*(3), 165-183.

Goutte, C., Toft, P., Rostrup, E., Nielsen, F. A., & Hansen, L. K. (1999). On clustering fMRI time series. *NeuroImage*, *9*(3), 298-310.

Howseman, A. M., Grootoonk, S., Porter, D. A., Ramdeen, J., Holmes, A. P., & Turner, R. (1999). The effect of slice order and thickness on fMRI activation data using multislice echo-planar imaging. *Neuroimage*, *9*(4), 363-376.

Jain, A. K., & Dubes, R. C. (1988). *Algorithms for clustering data*. Prentice-Hall, Inc..Jain, A. K. (2010). Data clustering: 50 years beyond K-means. *Pattern recognition letters*, *31*(8), 651-666.

Khairi, N. M., Wilkes, D. M., & Ding, Z. (2019, April). Modified Principal Component Analysis in sliding windowed fMRI data. In *2019 SoutheastCon* (pp. 1-6). IEEE.

Lange, N., & Zeger, S. L. (1997). Non-linear Fourier time series analysis for human brain mapping by functional magnetic resonance imaging. *Journal of the Royal Statistical Society: Series C (Applied Statistics)*, *46*(1), 1-29.

Lee, M. H., Smyser, C. D., & Shimony, J. S. (2013). Resting-state fMRI: a review of methods and clinical applications. *American Journal of neuroradiology*, *34*(10), 1866-1872.

Liu, X., Zhang, N., Chang, C., & Duyn, J. H. (2018). Co-activation patterns in resting-state fMRI signals. *Neuroimage*, *180*, 485-494.

Logothetis, N. K., Pauls, J., Augath, M., Trinath, T., & Oeltermann, A. (2001). Neurophysiological investigation of the basis of the fMRI signal. *nature*, *412*(6843), 150-157.

McKeown, M. J., Makeig, S., Brown, G. G., Jung, T. P., Kindermann, S. S., Bell, A. J., & Sejnowski, T. J. (1998). Analysis of fMRI data by blind separation into independent spatial components. *Human brain mapping*, *6*(3), 160-188.

Meilă, M. (2006, June). The uniqueness of a good optimum for k-means. In *Proceedings of the 23rd international conference on Machine learning* (pp. 625-632).

Metropolis, N., Rosenbluth, A. W., Rosenbluth, M. N., Teller, A. H., & Teller, E. (1953). Equation of state calculations by fast computing machines. *The journal of chemical physics*, *21*(6), 1087-1092.

Moser, E., Baumgartner, R., Barth, M., & Windischberger, C. (1999). Explorative signal processing in functional MR imaging. *International Journal of Imaging Systems and Technology*, *10*(2), 166-176.

Moser, E., Diemling, M., & Baumgartner, R. (1997). Fuzzy clustering of gradient-echo functional MRI in the human visual cortex. Part II: Quantification. *Journal of Magnetic Resonance Imaging*, *7*(6), 1102-1108.

Norman, K. A., Polyn, S. M., Detre, G. J., & Haxby, J. V. (2006). Beyond mind-reading: multi-voxel pattern analysis of fMRI data. *Trends in cognitive sciences*, *10*(9), 424-430.

Sychra, J. J., Bandettini, P. A., Bhattacharya, N., & Lin, Q. (1994). Synthetic images by subspace transforms I. Principal components images and related filters. *Medical Physics*, *21*(2), 193-201.

Toft, P., Hansen, L. K., Nielsen, F. Å., Hansen, L. K., Lange, N., Mørch, N., ... & Rostrup, E. (1997). On clustering of fMRI time series.

von Economo, C. F., & Koskinas, G. N. (1925). *Die cytoarchitektonik der hirnrinde des erwachsenen menschen*. J. Springer.

Wismüller, A., Dersch, D. R., Lipinski, B., Hahn, K., & Auer, D. (1998, September). A neural network approach to functional MRI pattern analysis—clustering of time-series by hierarchical vector quantization. In *International Conference on Artificial Neural Networks* (pp. 857-862). Springer, London.

Worsley, K. J., & Friston, K. J. (1995). Analysis of fMRI time-series revisited—again. *Neuroimage*, *2*(3), 173-181.

Xiong, J., Gao, J. H., Lancaster, J. L., & Fox, P. T. (1996). Assessment and optimization of functional MRI analyses. *Human Brain Mapping*, *4*(3), 153-167.

Yeo, B. T., & Ou, W. (2004). Clustering fMRI time series.